GEOLOGICA CARPATHICA, 2025, 76, 2, 137–152 https://doi.org/10.31577/GeolCarp.2025.12

Surface microtextures on detrital accessory garnets in the fluvial environment: Case study from an active stream (Malá Fatra Mts., Western Carpathians)

KATARÍNA BÓNOVÁ[1,✉], JÁN BÓNA[1,2], GABRIELA FABRICIOVÁ[3], TOMÁŠ MIKUŠ[4] and DUŠAN BARABAS[1]

[1]Institute of Geography, Faculty of Science, Pavol Jozef Šafárik University in Košice, Jesenná 5, 040 01 Košice, Slovakia
[2]DPP Žilina Ltd., Legionárska 8203, 010 01 Žilina, Slovakia
[3]Institute of Physics, Faculty of Science, Pavol Jozef Šafárik University in Košice, Jesenná 5, 040 01 Košice, Slovakia
[4]Earth Science Institute, Slovak Academy of Sciences, Geological Division, Ďumbierska 1, 974 01 Banská Bystrica, Slovakia

(Manuscript received March 6, 2025; accepted in revised form August 18, 2025; Associate Editor: Igor Broska)

Abstract: Surface analysis of detritus from a modern fluvial environment can be a useful tool in understanding various weathering and transport processes; the results of which are applicable in the provenance and environmental interpretations of ancient sedimentary rocks. In this study, we provide a report on the microtextural and geochemical relationships within detrital garnets hosted in modern fluvial sediments. Garnets from seventeen heavy-mineral concentrates taken from the Stránsky potok brook were analysed by optical microscopy, scanning electron microscopy, Raman spectroscopy, and electron microprobe to obtain information on their provenance and surface microtextural development. The results show that detrital almandines (1) $Alm_{57–72}Sps_{12–23}Prp_{10–15}Grs_{1–5}And_{0–1}$ and (2) $Alm_{66–77}Prp_{15–24}Sps_{3–9}Grs_{1–4}And_{0–1}$ were primarily sourced in local Variscan crystalline basement rocks, such as metagranite (diatexite) with gneiss xenoliths. A large part of recycled almandine was likely derived from the Permian Stráňany Formation (Fm.) and/or Triassic Lúžna Fm. siliciclastic rocks. Almandine recorded various transport traces, such as conchoidal fractures, arcuate and straight steps, V-shaped cracks and crescentic percussion marks formed in the (a) contemporary Variscan basement and (b) older fluvial environments. Chemically-induced features, such as facets developed on first-cycle almandines are a remnant after corrosion caused by acid solutions – resorption in the garnet rims interacted with other minerals during metamorphic events in the Malá Fatra Mountains, and the solution crevasses developed considerably on recycled grain surfaces formed by intrastratal dissolution. The investigation of detrital garnet in the recent stream of the Malá Fatra Mts. revealed (paleo)environmental and depositional conditions of sedimentation.

Keywords: Western Carpathians, Malá Fatra Mts., detrital garnet, scanning electron microscopy, surface microtextures, geochemistry

Introduction

Garnets are rock-forming in several common low-to-high grade metamorphic lithologies and are also present as accessory minerals in a wide range of igneous rocks. Garnet is therefore a common constituent of clastic detritus and is traditionally used in provenance research (Morton et al. 2005; Mange & Morton 2007; Morton et al. 2012; Krippner et al. 2014, 2015; Suggate & Hall 2014; Tolosana-Delgado et al. 2018; Hong et al. 2020; Schönig et al. 2021; Naidu et al. 2024); however, its precise discriminatory potential is occasionally complicated. Some studies noticed that geochemical composition of detrital garnet can be closely related to grain size, and this can affect provenance considerations (e.g., Krippner et al. 2015, 2016). Garnet is a moderate-stable heavy mineral and can degrade quickly by prolonged stay in the soil (Embrechts & Stoops 1982; Velbel 1984; Salvino & Velbel 1989; Andò et al. 2012). A compositional control on garnet diagenetic stability is also known and relates to a decrease in the Ca content of bulk garnet samples with burial depth and an increase in Fe content (Morton & Hallsworth 2007). Because Mn and Mg contents in that example remained unchanged, this could indicate higher diagenetic vulnerability of Ca-rich garnets, such as grossular, andradite, and uvarovite (Morton & Hallsworth 2007). Significant destruction of detrital garnet can occur even in the first sedimentary cycle in a fluvial environment (Bónová et al. 2024b). In view of these facts, it is necessary to continue the detailed investigation of garnet.

Based on the study by Malusà's et al. (2016), the heavy-mineral content of detrital fluvial sediment produced in proximal catchments sensitively reflects source rock fertility if the heavy-mineral spectrum is not modified during transport or deposition. However, many factors, such as hydraulic sorting, grain shape, geochemistry, density, size, weathering grain stage, climate conditions, grain texture, transport medium, recycling (Morton et al. 2005; Morton & Hallsworth 2007; Garzanti et al. 2008, 2009, 2018; Feil et al. 2024), and separation approach (Vermeesch 2004; Chew et al. 2020; Stutenbecker

✉ corresponding author: Katarína Bónová
katarina.bonova@upjs.sk

et al. 2024) may significantly affect the resulting heavy-mineral concentrates.

In this paper, the surface microtextural features and chemical composition of the detrital garnet from modern fluvial sediments are discussed with the objective of providing constraints on its origin in source rocks, as well as its utility as an indicator of transport processes in the fluvial environment. The research has a relatively local character when considering the analysis of sediments taken from an approximately 9 km-long section of the Stránsky potok brook located in the crystalline massif of the Malá Fatra Mts. in the Western Carpathians (Fig. 1). Nevertheless, this type of area is ideal for investigating the behaviour of garnets in a fluvial environment, as well as in relation to the local water-flow conditions. The findings can be beneficial for the evaluation of the detritus nature from the ancient sediments/sedimentary rocks and for the correct identification of transport conditions, which are "imprinted" into the heavy-mineral surfaces. In other words, surface features on detrital minerals are crucial for inferring the paleoenvironmental conditions. Their morphology, abrasion degree, and various microtextural patterns can reveal transport history, sedimentary processes, and the energy levels of the depositional environment (Garzanti et al. 2015; Nascimento et al. 2022; Ma et al. 2024). Garnet appears especially promising in this regard (e.g., Bónová et al. 2024a, b; Delgado et al. 2025).

Geological and geomorphological framework of the study area

Geologically, the Malá Fatra Mts. are an integral part of the Tatric megaunit belonging to the Inner Western Carpathians (Hók et al. 2019) and are located in the northern-western part of Slovakia (Fig. 1A). Their crystalline basement consists of relatively large, monotonous granitoid pluton with complicated poly-phase evolution (Kamenický et al. 1987; Broska et al. 1997, 2022; Dianiška et al. 2002; Faryad & Dianiška 2003; Hrdlička 2006; Kurylo & Broska 2025) and diverse high-grade metamorphic rocks, such as paragneisses, migmatites, amphibolites, and amphibolite gneisses (Geological map 2008; Fig. 1B). The Variscan (353±5 – 342±3 Ma) age of the Malá Fatra Mts. granitoids was established by U–Pb zircon dating (Shcherbak et al. 1990; Hrdlička 2006; Broska & Svojtka 2020; Kohút & Larionov 2021; Broska et al. 2022). Some crystalline rocks contain garnet. Almandine garnet occurs in granodiorite (metagranite, diatexite: $Alm_{66–71}Prp_{12–19}Sps_{4–19}Grs_{2–8}$; Hrdlička 2006), in garnet–sillimanite paragneiss ($Alm_{65–75}Prp_{15–30}Sps_{2–6}Grs_{3–7}$), and in garnet–clinopyroxene amphibolite ($Alm_{59–63}Prp_{10–12}Sps_{2–5}Grs_{23–25}$; Méres & Hovorka 1989; Janák & Lupták 1997; Hovorka et al. 2008). Faryad & Dianiška (2003) described andradite-rich garnets ($Adr_{50–74}Grs_{32–42}$schorlomite+morimotoite$_{1–14}$) in various granitoids as a product of their post-magmatic cooling. Hrdlička (2006) confirmed a similar composition of secondary garnet ($Grs_{7–51}Adr_{40–92}Scho_{0–8}$) in tonalite. The crystalline basement is locally covered by the Late Paleozoic, Mesozoic, and Cenozoic sedimentary rocks.

The study area is located in the north-western part of the Veľká Lúka segment within the Stránsky potok brook catchment (Fig. 1A–C), in which tonalite commonly transits to granodiorite and includes local lenses of gneisses and amphibolite (Geological map 2008). In addition, spinel and olivine-bearing metaultramafite (without garnet) was documented on the top of the Veľká Lúka segment (Hovorka et al. 1985; Korikovsky et al. 1998). The sedimentary succession cover in the Stránsky potok brook catchment area is represented by the Permian Stráňany Formation (Fm). and Lower Triassic Lúžna Fm.; both consist of siliciclastic rocks. Provenance of these formations have been discussed in numerous studies. While the Stráňany Fm. siliciclastics were derived from local crystalline basement rocks (Vozárová & Vozár 1983, 1988); the source for the Lúžna Fm. sedimentary rocks is still unclear (Fejdiová 1985; Hók 1989; Mišík & Jablonský 2000; Vozárová et al. 2003).

Geomorphologically, the Stránsky potok brook catchment area is located from the Krížava elevation (1457 m a.s.l.) in the east, to the western part of the village of Poluvsie, near the confluence of the Stránsky potok and Rajčianka brooks at 394 m a.s.l. The studied catchment is delimited by 1180-m and 1015-m high escarpments around its northern boundary, and elevations of 1304-m and 1006-m are found on its southern boundary. The highlands in the eastern part of the study area correspond with uplifted granitoid pluton and metamorphic basement rocks, whereas the western part forms an anticline (the Kozol anticline; for details, see Rakús & Hók 2003; Havrila & Olšavský 2015) with a core of the Permian formations rimmed by the Triassic siliciclastic rocks (Fig. 1B). The surrounding confluence is filled by Quaternary proluvial, deluvial, and fluvial sediments.

Methods

Sampling

Seventeen samples of modern fluvial sediments were taken at relatively regular intervals in the Stránsky potok brook from its source almost to its confluence with the Kunerádsky potok brook. The sampling locations are listed in Table 1 and depicted in Fig. 1B. Samples weighing approximately 2.5 kg were taken, then finely-panned to obtain the heavy-mineral concentrates. The concentrates were then studied under a LEICA M80 stereomicroscope. We focused mainly on garnet and partially on amphibole. After the sample quartering, randomly-selected grains of different sizes, shapes, and colours were separated for further morphological, microtextural, and geochemical study. Samples of surrounding potential source rocks intended for comparative purposes were evaluated macroscopically in the entire stream profile; some of them intended for a microscopic study were taken from the centre of the Stránsky potok brook channel (MFB-12A–D;

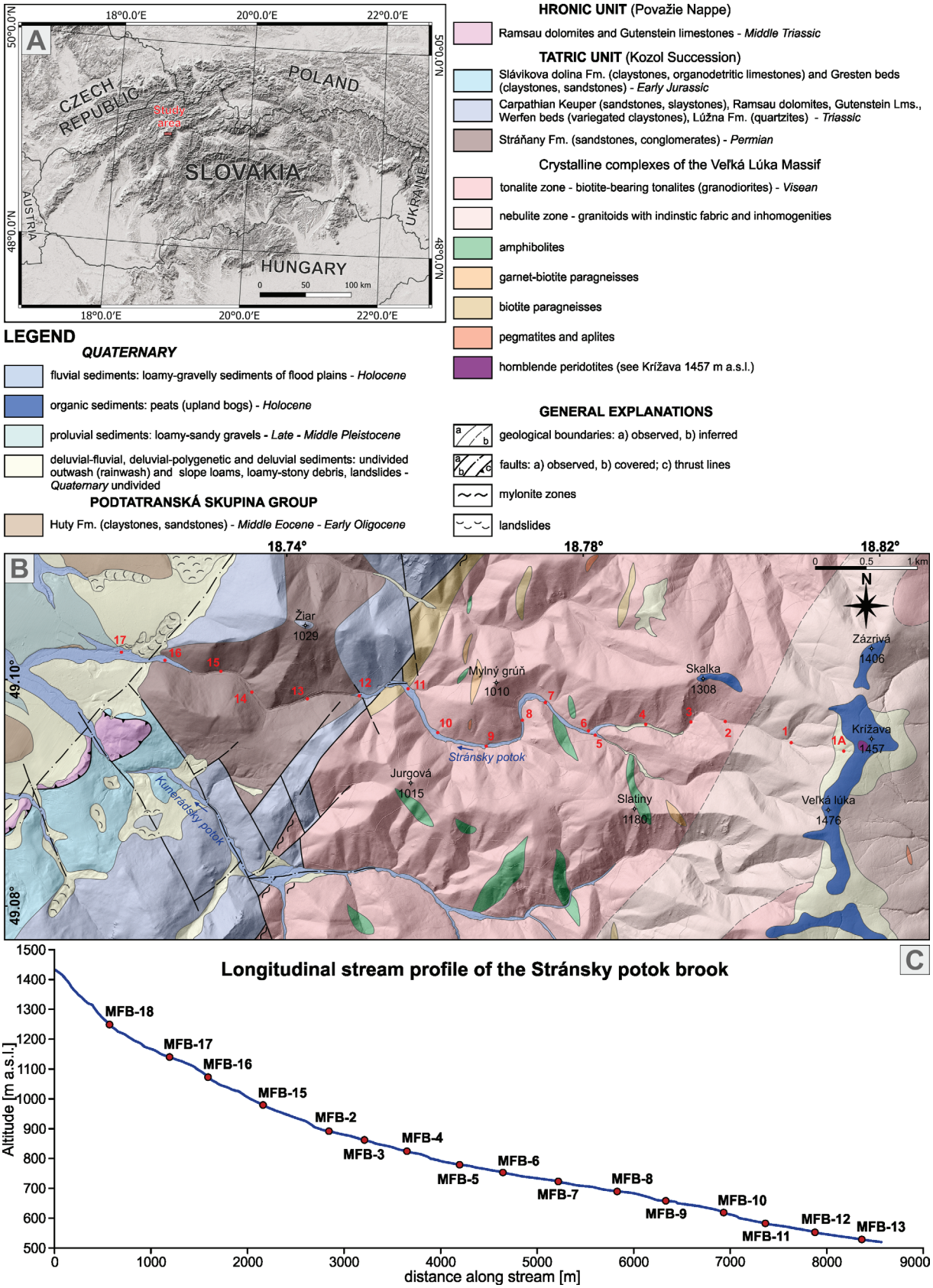

Fig. 1. **A** — Position of the studied area in Central Europe. **B** — Geological sketch map of the western part of the Malá Fatra Mts. (according to Rakús et al. 1993; Hrdlička 2006; Geological map 2008; Havrila & Olšavský 2015; Broska et al. 2022) with sample locations. **C** — Longitudinal stream profile of the Stránsky potok brook.

Table 1: Geographic coordinates (WGS 84) of the fluvial samples studied. Water-flow velocity and depth are also listed. *A comparative sample.

No.	Sample	Coordinates		Altitude m.s.l.	Gravels	Water-flow velocity (max)	Water-flow velocity (average)	Depth (cm)
		GPS N	GPS E					
1A	MFB-Kr	49°05.751’	18°48.988’	1439	metaperidotite	–	–	–
1	MFB-18	49°05.785’	18°48.502’	1250		0.9	0.1	10
2	MFB-17	49°05.887’	18°47.970’	1133		0.8	0.2	24.5
3	MFB-16	49°05.877’	18°47.692’	1060	granodiorite tonalite amphibolite	2.3	0.6	10
4	MFB-15	49°05.860’	18°47.333’	979	granodiorite tonalite amphibolite	1.7	0.4	11
5*	MFB-1	49°05.815’	18°46.870’	900		–	–	–
6	MFB-2	49°05.815’	18°46.862’	897		3.5	1.2	17
7	MFB-3	49°05.978’	18°46.527’	862		1.9	0.4	18
8	MFB-4	49°05.861’	18°46.335’	820		0.8	0.6	13.5
9	MFB-5	49°05.722’	18°46.050’	780	amphibolite	3.2	0.6	16
10	MFB-6	49°05.785’	18°45.657’	748	amphibolite	1.6	0.3	15.5
11	MFB-7	49°06.007’	18°45.401’	718		1.1	0.2	26
12	MFB-8	49°05.964’	18°45.012’	692		2.7	0.9	26
13	MFB-9	49°05.946’	18°44.597’	655	arkose (up to 30 cm)	1.9	0.7	15
14	MFB-10	49°05.974’	18°44.154’	618	sandstone arkose	1.9	0.3	27
15	MFB-11	49°06.079’	18°43.890’	583		2.7	0.9	18.5
16	MFB-12	49°06.137’	18°43.446’	551	tonalite amphibolite arkose biotite paragneiss	1.9	0.7	7
17	MFB-13	49°06.159’	18°43.086’	524		1.5	0.6	8

MFB-6 and MFB-Kr samples). Polished thin sections were prepared in the laboratories of the Earth Science Institute of the Slovak Academy of Sciences in Bratislava, Slovak Republic (ESI SAS) and examined under a Leica DM 2500 P polarizing microscope.

Scanning electron microscopic analysis

The TESCAN VEGA-3 XMU Scanning Electron Microscope (SEM) at 20–30 kV and 1 nA at the UPJŠ Institute of Physics was used for visualization of detrital grain’s surfaces. Detrital grains from 17 fluvial samples were fixed on a double-stick carbon sticker, and approximately 30 grains from each sample were analysed by back scattered electron microscopy. The frequency of various microtextures observable using SEM was calculated by their counting on the individual grain surfaces from all samples studied. The surface microtextures were classified according to Mahaney (2002), Moral Cardona et al. (2005), Krinsley & Doornkamp (2011), Vos et al. (2014), Finzel (2017), Linnemann et al. (2018), Szerakowska et al. (2018), Armstrong-Altrin (2020), Armstrong-Altrin et al. (2022), and Bónová et al. (2021, 2024a, b).

Microchemical analysis (EMPA)

The chemical analysis of garnet taken from the fluvial sediments was performed to obtain the chemical composition, as well as to identify the trapped mineral inclusions. Garnet geochemistry provided by JEOL JXA 8530FE wavelength-dispersive electron probe microanalyser at the ESI SAS in Banská Bystrica, Slovak Republic at the following conditions: accelerating voltage 15 kV, probe current 20 nA, beam diameter 2–3 µm, ZAF correction, counting time 10 s on peak, 5 s on background. X-ray lines and detection limits (in ppm) for the standards used are: Ca (Kα, 25) – diopside, Na (Kα, 43) – albite, Mg (Kα, 41) – olivine, Al (Kα, 42) – albite, Si (Kα, 63) – quartz, Fe (Kα, 52) – hematite, Cr (Kα, 113) – Cr2O3, Mn (Kα, 59) – rhodonite, V (Kα, 117) – ScVO4, Ti (Kα, 130) – rutile, and Zn (Kα, 150) – willemite. The representative chemical analyses are listed in Electronic Supplement S1. Crystallochemical formulae were calculated by Grew’s et al. (2013) and end-members according to Locock’s (2008) procedures. In addition, we analysed the amphiboles by the same instrument and the obtained analytical results were normalised by Locock’s (2014) procedure and then classified according to Hawthorne’s et al. (2012) amphibole classification. The chemical composition of pyroxene and spinel from metaultramafite was also determined.

Raman spectroscopy

All Raman spectra were obtained using a Raman confocal microspectrometer (Renishaw inVia, Great Britain) equipped with a Leica upright microscope, an electrically cooled CCD camera, and an 1800 lines/mm diffraction grating at the UPJŠ Institute of Physics. The system was calibrated and monitored

using a silicon reference (520.5 cm^{-1}) before measurements. The laser beam operated at a wavelength of λ=532 nm (Cobolt CW DPSS laser). Spectra from detrital grains of the MFB-18 sample were recorded over the wavenumber range of 100–4000 cm^{-1}, with the sample focused using a 100× microscopic objective (NA 0.9; laser spot diameter ~1 μm). The spectral resolution was 1 cm^{-1}. The accumulation time for a single spectrum was 10 s, with one accumulation collected for each measurement area. Spectra from the MFB-12A sample were recorded in two spectral regions: 100–1800 cm^{-1} and 2800–4000 cm^{-1}. Collection times for Raman spectra in the low-frequency region involved 20 accumulations of 5 s each, while the high-frequency region used 65 accumulations of 5 s each. At least five measurement points were selected on each garnet.

Longitudinal stream profile and stream-flow velocity

In order to accurately assess the influence of the Stránsky potok brook flow dynamics on the destruction of heavy-mineral detritus better, the flow velocity and water depth were measured in the individual sampling sites copying the longitudinal stream profile from the spring (below Krížava elevation 1457 m a.s.l.) to Kunerad village (524 m a.s.l.). At each sampling point, the position of which was determined by GPS, the maximum water flow velocity at the point of the streamline, and the maximum depth of the transverse profile were measured by a hydrometric wing (Global Water FP 111). The mean flow velocity in the transverse profile of the channel was evaluated. Hydrological measurements were carried out once in June, 2022. The measured values are listed in Table 1.

In addition, we exported the coordinates and elevation data to Microsoft Excel in which the longitudinal stream profile was processed. We constructed a height longitudinal profile (in metres) to identify possible changes and to better visualise the potential anomalies (knickpoints) in the studied profile (Fig. 1C).

Results

Petrography of gravels (source rocks)

In the set of the analysed gravels, granodiorite/tonalite (~90 %) are the most common. In addition to granitoids, amphibolite (~8 %), biotite paragneiss, arkose, sandstone, and limestone (~2 %) were found. Locally, we observed metaperidotite in the area just below the source of the Stránsky potok brook. The gravel size ranges between ~1.5 and 9 cm, occasionally more (~30 cm). The petrographic (macroscopic) character of the gravels taken from the sampling points is listed in Table 1.

Granodiorite/tonalite clasts are macroscopically medium- to coarse-grained rocks with a massive texture. The mineral assemblage consists of strongly-sericitised and saussuritised plagioclase, which significantly prevails over sporadic K-feldspar (K-feldspar occurs chiefly in granodiorite). Plagioclase is represented by two generations: an older, tiny, allotriomorphic plagioclase is intensely sericitised, while the younger hypidiomorphic one encloses the older plagioclase generation, which is explained by Kurylo & Broska (2025) as intense Variscan mixing processes. Xenomorphic, undulose quartz usually fills interstitial spaces. Sericitised and kaolinised K-feldspars are allotriomorphic, often interstitial, and encompass plagioclase, quartz and biotite. Hypidiomorphic to xenomorphic, strongly-chloritised and locally-baueritised biotite encloses rutile, apatite, rarely zircon. Amphibole in tonalite is often associated with secondary garnet, and in some places, the contact among both minerals is relatively sharp. Somewhere, the amphibole is trapped in primary titanite (Fig. 2A). Based on Hawthorne's et al. (2012) classification, the analysed amphiboles (inclusions and interstitial crystals) correspond to magnesio-hastingsite (X_{Mg}=~0.59), sporadically altered to actinolite. Accessory minerals are apatite, zircon, allanite, titanite, magnetite, and ilmenite. Generally, magnetite prevails over ilmenite in tonalite. Titanite forms fine inclusions in feldspars, locally in quartz. Secondary minerals (such as late hydrothermal alteration products or Alpine tectonothermal ones) are rutile, garnet, titanite II, and chlorite. Secondary titanite is rarely incorporated in biotite/chlorite cleavage. Secondary garnet is an anhedral and intergrown with chlorite, epidote, or amphibole.

Amphibolite clasts are grey-black-green in colour, as well as massive and fine- to medium-grained, with a distinctly linear texture. The mineral association consists of amphibole, plagioclase, biotite, quartz, epidote, and garnet. Amphibole is chloritised and epidotised. Plagioclase tends to be significantly sericitised, saussuritised, and often broken. Biotite is chloritised, baueritised, and locally contains hematite coatings. Quartz is rather rare and undulose. Zircon, apatite, titanite, ilmenite, pyrite, and K-feldspar are accessory minerals; garnet and epidote are secondary ones. Secondary garnet forms aggregates with amphibole, chlorite and apatite. Based on Hawthorne's et al. (2012) classification, the amphiboles correspond to magnesio-hornblende locally with actinolitic rims (X_{Mg}=0.64–0.66, X_{Mg}=0.73–0.80, respectively). These rims and epidote presence indicate greenschist-facies retrogression.

Metaultramafite (metaperidotite) clasts are dark green massive rocks whose composition includes olivine, amphibole, orthopyroxene, spinel, magnetite, and chlorite. The proportion of olivine (Fo78) sometimes reaches 65 %. In many places, there are serpentine micro-veinlets formed as a part of olivine alteration. Sporadic orthopyroxene compositionally corresponds to enstatite ($En_{80}Fs_{19}Wo_{\sim 0.5}$) and is either trapped in amphibole (Fig. 2B) or is locally present as porphyroblast. Amphibole, based on Hawthorne's et al. (2012) classification, corresponds to magnesio-hornblende and, to a lesser extent, magnesio–ferri-hornblende (X_{Mg}=0.93–0.96); however, its composition is different in comparison with magnesio-hornblende from tonalite (Fig. 3). Spinel ($Spl_{58}Hc_{36}Mfr_{\sim 2}Mag_{\sim 1}$) is often intimately intergrown with the mentioned minerals.

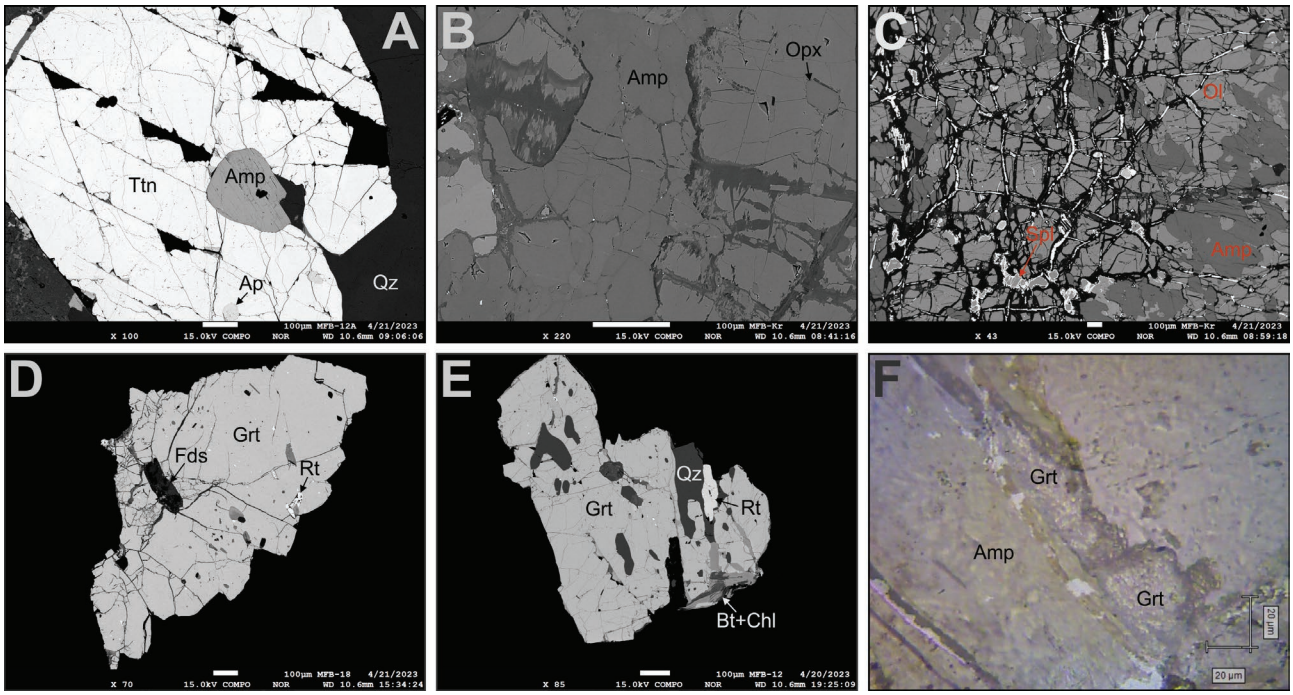

Fig. 2. BSE images: **A** — amphibole inclusion in primary titanite within tonalite; **B** — orthopyroxene trapped in amphibole within metaperidotite; **C** – spinel intimately intergrown with olivine and partly replaced by magnetite along its margins in metaperidotite; **D, E** — unzoned almandine with numerous inclusions and fractures filled by chlorite from the fluvial sediments; **F** — secondary hydrogarnet in tonalite (Raman microscopy image). Abbreviations from Warr (2021).

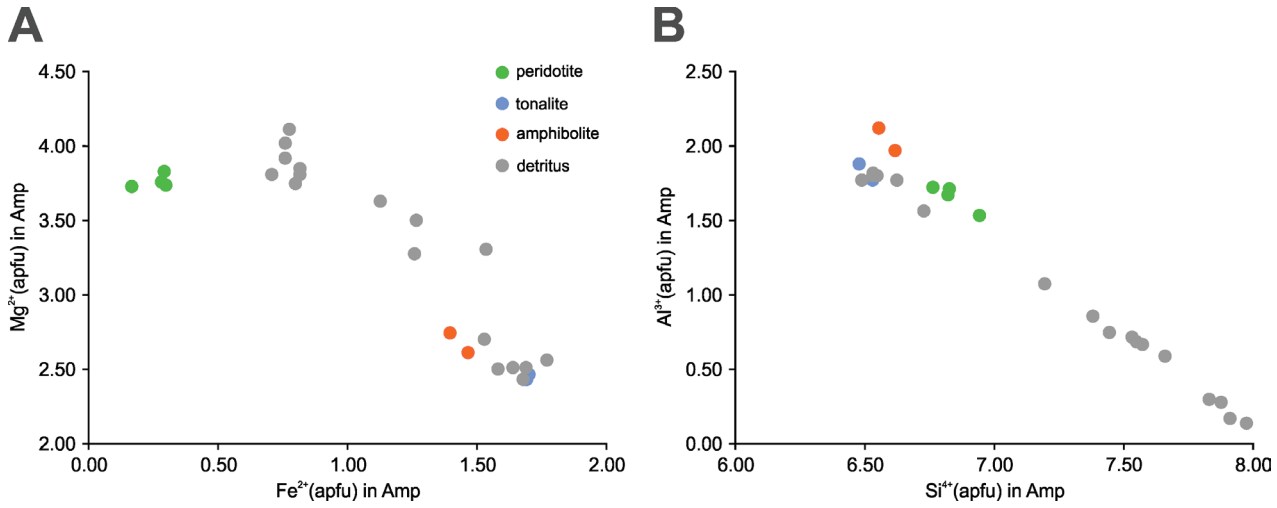

Fig. 3. Composition of detrital amphiboles compared to local amphibole sources (gravels) in Mg^{2+}/Fe^{2+} (**A**) and Al^{3+}/Si^{4+} (**B**) diagrams.

Its periphery is fully replaced by magnetite (Fig. 2C). The rock contains no garnet.

Sandstone clasts are a mixture of quartz, K-feldspar, plagioclase, baueritised biotite and lithic granitic fragments. Rare zircon and apatite were observed, while garnet wasn't at all.

Sporadic **biotite paragneiss** clasts consist mainly of sericitised plagioclase, K-feldspar, undulosed quartz and chloritised biotite. Muscovite is rather rare. Apatite, zircon, amphibole, magnetite, and monazite are accessory minerals; garnet was not observed.

Heavy-mineral assemblages of the fluvial sediments

The composition of the studied heavy-mineral concentrates does not principally change. They mostly contain garnet and amphibole; apatite, zircon, rutile, monazite, allanite, epidote,

and titanite are found in a smaller amount. Tourmaline and staurolite occur rarely in the MBZ-12 and MBF-8 samples, respectively. From the opaque minerals, magnetite is abundant, ilmenite is less common, and pyrite was rarely found. A slightly increased concentration of opaque minerals was recorded in the MFB-2, MFB-3 and MFB-4 samples. Under a stereomicroscope, the dominant garnets are clearly distinguishable in colour. Broken garnet grains of various pink shades unambiguously prevail in the concentrates. Olivine and spinel have not been observed.

Garnet geochemistry (EMPA) and Raman spectroscopy

Garnet in the host (gravel) rocks

Almandine garnet was not observed in our granodiorite thin sections. Sporadic secondary garnet from tonalite corresponds to grossular-andradite with low analytical sums of oxides indicating the presence of a hydroxyl component (Hrdlička 2006).

The secondary garnet in the MFB-12A sample (tonalite) was analysed using Raman spectroscopy. In the range 100–1200 cm^{-1}, the Raman spectra of garnets are usually divided into two regions: external vibrations below 400 cm^{-1} and internal vibrations above 400 cm^{-1} (Kolesov & Geiger 1998). The external vibrations, up to 320 cm^{-1}, are attributed to SiO_4 tetrahedra and divalent cations translation, and between 320–400 cm^{-1} to the liberations of SiO_4 units. In the region related to internal vibrations, between 400 cm^{-1} and 650 cm^{-1}, O–Si–O bending modes are present, and at frequencies higher than 800 cm^{-1}, one can observe the Si–O stretching modes.

Analysis of the Raman spectrum in the high-frequency range (above 3000 cm^{-1}) allows the presence of OH groups in samples to be determined.

Raman spectra were recorded from 100 cm^{-1} to 1200 cm^{-1} and from 3400 cm^{-1} to 3900 cm^{-1}. The bands which are characteristic of the molecular composition were observed in the region 100–1200 cm^{-1}, and structural/hydration water bands (both H_2O and OH groups) occur in the 3000–3700 cm^{-1} region.

Figure 4A presents the characteristic Raman spectrum in the region 100–1200 cm^{-1}. The profile of the spectrum corresponds to andradite (Bersani et al. 2009; Enami 2012; Fu et al. 2022). The most significant change observed between the published spectra of andradite (andradite molecule in these samples is more than 80 mol%) and the spectrum in Figure 4A is in the intensities of the bands in the region 800–900 cm^{-1}. The most intense Raman band in this region for andradite is located above 860 cm^{-1}; the remaining two have significantly lower intensities (Bersani et al. 2009; Enami 2012; Fu et al. 2022). In the Raman spectrum of the MFB-12A sample (Fig. 4A), the intensities of the bands at 816 and 875 cm^{-1} differ only slightly, and the band at 843 cm^{-1} shows the lowest intensity. A similar spectrum to ours is presented in the work of Fu et al. (2022), in which Raman spectra of garnets belonging to the andradite-grossular solid solution series are depicted. A similar spectrum to that in Figure 4A corresponds to garnet containing about 56 mol% andradite and 25 mol% grossular. Similar Raman spectra were also obtained by Butek et al. (2021) when studying garnets belonging to the grossular–andradite series. Based on the positions of the bands in the spectrum in Figure 4A, we can assume that andradite and grossular are present in our sample as well.

In the Raman spectrum (Fig. 4B), we can observe the internal OH-stretching modes. This spectrum has a very low intensity compared to the spectrum in the region 100–1200 cm^{-1}; therefore, it is enlarged for better interpretation. In the Raman spectrum above 3400 cm^{-1}, we observed a prominent band at 3645 cm^{-1}, in addition to two bands with lower frequency (3618 and 3578 cm^{-1}) and a band at 3579 cm^{-1}. In the region of 3500–3750 cm^{-1}, Raman bands were also observed in the spectra of garnets belonging to the grossular–andradite series, demonstrating the different degree of hydration of these samples (Butek et al. 2021). Thus, in the spectrum in Figure 4B, we observed bands corresponding to OH stretching vibrational modes of hydrated garnets. Kyono & Arora (2019) studied the synthesized hydrogrossular crystals by Raman spectroscopy. They observed a band at 3650 cm^{-1}, which corresponded to OH stretching vibrations and, in addition, a band at 3580 cm^{-1}, which was related to the substitution of Si for H. However, in the spectrum in Figure 4B, we observed a higher degree of complexity. This may be due to multi-site OH substitution in crystals, whose chemical composition is more complex, and/or they have more and different kinds of defects.

Based on these results, we assume that the secondary garnet from the MFB-12A sample is a hydrogarnet, which contains, in addition to andradite, a certain amount of hydrogrossular (Lager et al. 1989; Diella et al. 2019; Kyono & Arora 2019; Butek et al. 2021).

Garnet in the fluvial sediments

Based on a detailed EMPA study, the heavy-mineral suites contain almandine in all samples studied. Almandine is either (1) slightly zoned with medium spessartine content ($Alm_{57–72}Sps_{12–23}Prp_{10–15}Grs_{1–5}And_{0–1}$) or (2) unzoned with relatively stable content of the individual garnet components and a low spessartine content ($Alm_{66–77}Prp_{15–24}Sps_{3–9}Grs_{1–4}And_{0–1}$). We rarely found garnets with a slightly higher grossular molecule in contrast to the previous almandine ($Alm_{52–55}Prp_{18–20}Sps_{13–16}Grs_{11}And_{1}$) in the MFB-5 sample. Zircon, rutile, apatite, monazite, mica, and quartz are enclosed in almandine grains. Chlorite occasionally fills the fractures in the largest highly fractured grains (Fig. 2D, E). In addition to the mentioned inclusions, K-feldspar and ilmenite sporadically occur in almandine with a higher spessartine content. The chemical composition of the garnets studied is depicted in Figure 5.

Raman spectra of two representative garnet grains (from the MFB-18 sample) are shown in Figure 4C. These grains partially differ in the ratios of their components (end-members) as mentioned above. However, in both grains, almandine is the predominant component (more than 60 mol%), which is reflected in the bands observed in the Raman spectra of each

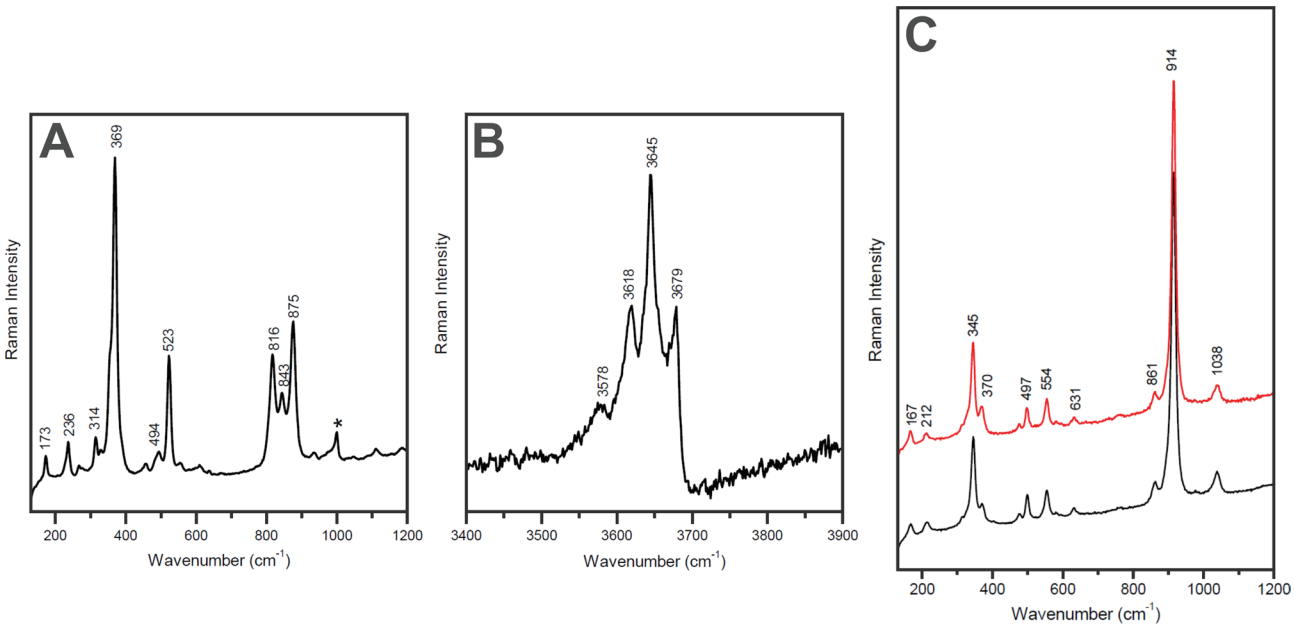

Fig. 4. Representative unpolarized Raman spectra of hydrogarnet from the MFB-12A sample (tonalite) in two considered ranges of frequency: (**A**) 130–1200 cm^{-1} and (**B**) 3400–3900 cm^{-1}, band at 1001 cm^{-1} (asterisk) comes from resin; and of (**C**) detrital almandine from the MFB-18 sample with a high spessartine content (black) and low spessartine content (red) in a low frequency region.

grain (Enami 2012; Kos et al. 2020). Black Raman spectrum in the Figure 4C was obtained from the garnet containing mainly almandine (62–64 mol %), spessartine (18–21 mol %), and pyrope (13–16 mol %). Red Raman spectrum corresponds to a garnet with a higher almandine content (70–74 mol %); additionally, the pyrope content is slightly higher (17–22 mol %) than in the previous grain, but the spessartine content is significantly lower (3–5 mol %). Despite changes in the chemical composition of these garnets, both spectra do not have only the same profile, but also the positions of the bands in the spectra remain almost unchanged, with only very slight variations in the intensities of some bands being noticeable.

Garnet shape and surface microtextures

Figure 6 depicts the recognised microtextural percentage abundance in the detrital almandine. In general, almandine garnets are usually angular in shape (~70 % occurrence), less subangular (up to 40 % occurrence in the MFB-10 sample), and rarely rounded (max. 13 % occurrence in the MFB-5 sample) with low to medium relief.

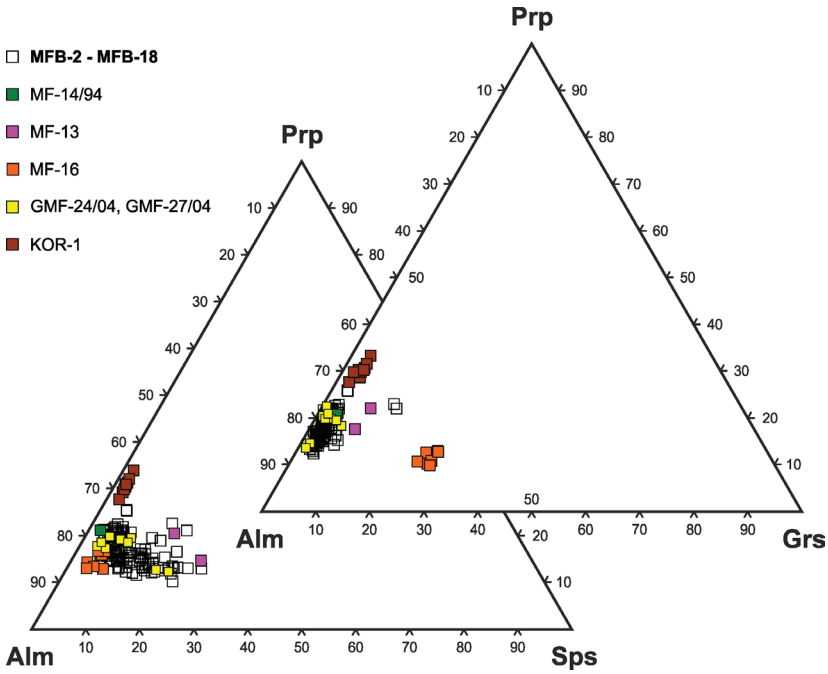

Fig. 5. Composition of the studied detrital garnets (MFB-2 – MFB-18) in Alm–Prp–Sps/Alm–Prp–Grs diagrams. Garnet compositions from the gneisses (MF-14/94, MF-13), amphibolites (MF-16; Janák & Lupták 1997), garnet–biotite gneisses (KOR-1; Korikovsky et al. 1987) and granodiorites (GMF-24/04, GMF-27/04; Hrdlička 2006) from the Malá Fatra Mts. crystalline basement are depicted for comparison.

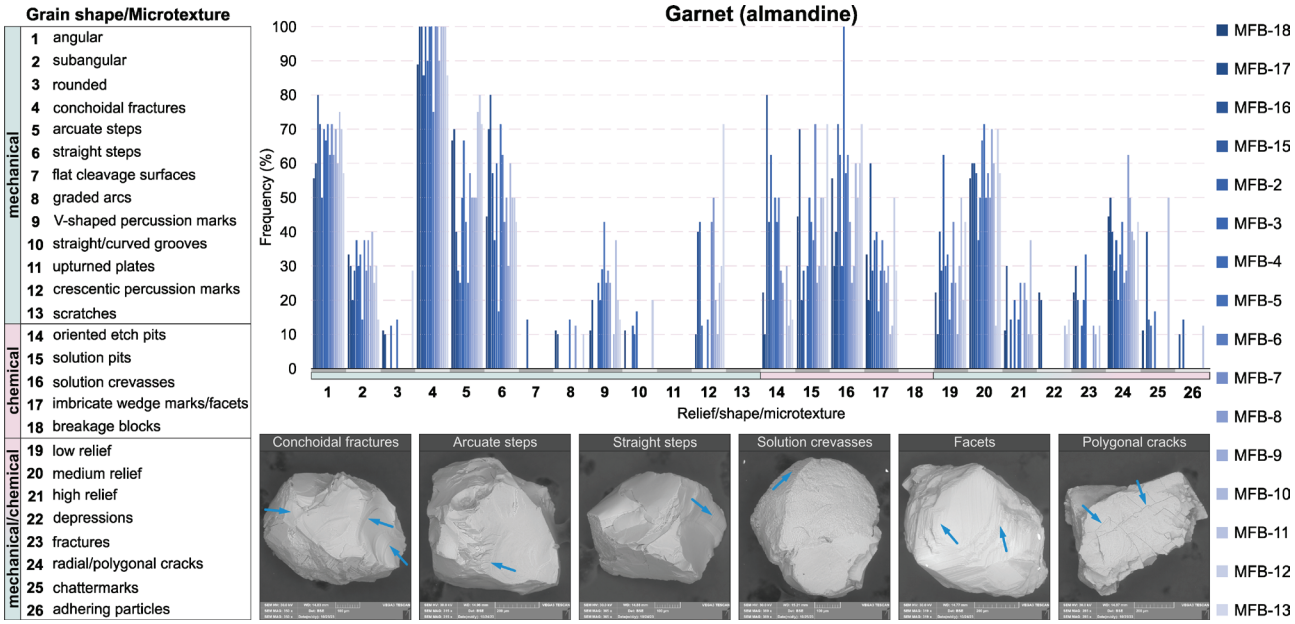

Fig. 6. Frequency (in %) of mechanical, chemical and combined mechanical/chemical microtextures on the detrital garnet surfaces studied with some representative examples.

Almandine is either covered by numerous solution pits (up to ~71 % occurrence), oriented etch pits (up to 80 % occurrence), solution crevasses (100 % occurrence; Figs. 6 and 7A, B) or, more rarely, by facets (Fig. 7C). Such strongly-etched garnet still has relatively sharp edges, and the mechanical features are loaded on its surface. Some grains, mainly from the MFB-2 sample, do not have any mechanical traces after fluvial transport; they involve dissolved surface and numerous traces after inclusion outage (Fig. 7D). Although the solution pits/oriented etch pits are usually absent on freshly broken surfaces, they were exceptionally observed in the MFB-13 sample (Fig. 7E). In addition, we evaluated the possible relationship between the occurrence frequency of individual, chemically-induced features in almandine surfaces. While the solution pits and oriented solution pits show medium dependence between them and facets (r=−0.53 and 0.44, respectively), there is almost no correlation between solution crevasses and facets (r=−0.18; Table 2).

Mechanical features occur more frequently against chemically-induced ones on almandine surfaces. There are common conchoidal fractures (up to 100 % occurrence) with arcuate and straight steps (Fig. 7F). V-shaped cracks are patchily developed on the conchoidal fractures (Fig. 7G). Crescentic percussion marks (Fig. 7H, I) occur almost on all analysed grains and are predominantly pronounced in the MFB-13 sample (71 % occurrence; Fig. 6). Tiny holes resembling the solution pits are remnant after the inclusion outage (Fig. 7J). Among the occurrences of frequencies of the individual mechanical features, no observable statistical dependence exists (Table 3). The table also highlights non-significant dependence among conchoidal fractures, arcuate steps, V-shaped percussion marks (r=0.34 and r=0.26, respectively), and, surprisingly, no relation between the conchoidal fractures and straight steps (r=−0.01). In relation to the appearance of mechanical microtextures on the almandine surface and water-flow velocity, a certain connection can be established between arcuate steps, conchoidal fractures, and water-flow velocity (other mechanical microtextures and hydrological characteristics of the stream show rather weak correlations among themselves, Table 3). In addition, various diatoms were observed on these almandine surfaces (Fig. 7K).

Almandine enriched in a spessartine molecule is rather rounded with low to medium relief and strongly-fractured, whilst the fractures are filled by secondary minerals (Fig. 7L). The grains show strongly-corrosive features, such as the oriented etch pits, solution crevasses (both up to 100 % occurrence), and facets.

With regards to the mechanical features, the conchoidal fractures combined with arcuate and straight steps strongly prevail over the V-shaped percussion marks. The latter were observed only on one grain.

Due to a small number of the analysed spessartine-rich almandine grains, a correlation analysis was not performed.

Characteristics of the Stránsky potok brook

The Stránsky potok brook has an elevation gain of 933 m and mean slope of 6.2° in the evaluated stream section. The slope value corresponds to the plan-view pattern, which, as a rule, does not create turns only with minor exceptions (Fig. 1). The stream belongs to the incised stream category. This corresponds to the local presence of the Quaternary

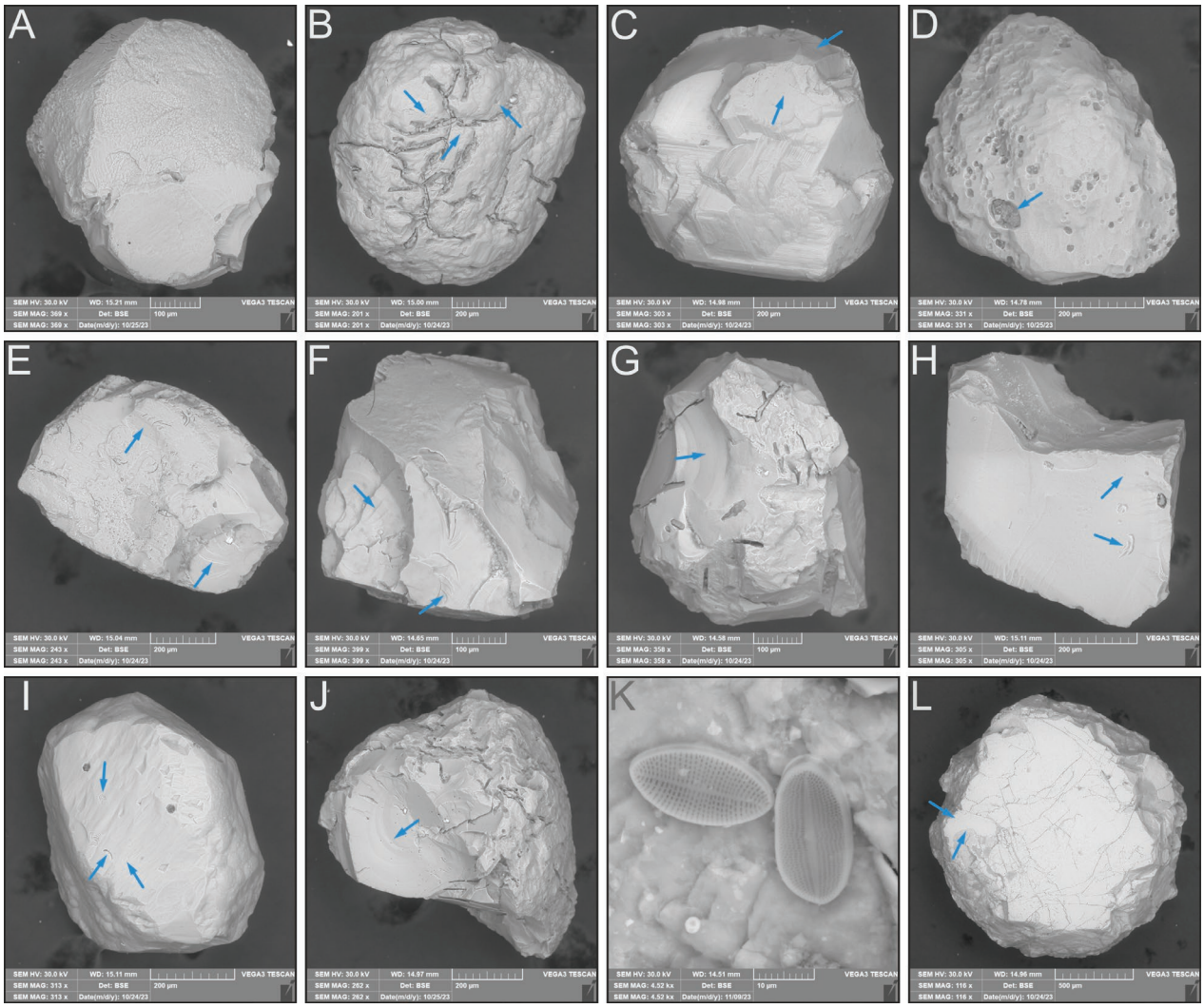

Fig. 7. SEM images of etched detrital almandine with solution pits/oriented etch pits (**A**); solution crevasses and crescentic percussion marks (**B**); V-shaped marks and straight steps (**C**); **D** — almandine grain with dissolved surface and traces after inclusion outage; **E** — broken almandine fragment with conchoidal fractures covered by tiny solution pits; **F** — conchoidally fractured almandine with arcuate and straight steps; **G** — conchoidally fractured grain with V-shaped percussion marks; **H** — almandine fragment with crescentic percussion marks, **I** — etched grain with loaded V-shaped percussion marks, crescentic percussion marks and chattermarks; **J** — broken fragment of the etched almandine with conchoidal fractures covered by tiny holes corresponding to remnant after the inclusion outage; **K** — diatoms attached to almandine; **L** — strongly-fractured, rounded spessartine-rich almandine with V-shaped marks. Arrows indicate the mentioned microtextures.

alluvium. The exception is the floodplain in the section between MFB-7 and MFB-8 sampling points, in such part of the longitudinal stream profile where a maximum water depth can be observed. The maximum water-flow velocities in the measured locations of MFB-2, MFB-5, MFB-8, MFB-11 and MFB-16 samples are the result of a higher slope of the riverbed in front of the measured section, or directly in the measured section (Fig. 1C). This is similarly reflected in the mean velocity values of the water flow. A certain dependence can also be observed in the measured depths – the points with a higher water-flow velocity show a relatively smaller water depth. Toward the downstream, these locations are followed by sites with a greater depth, which is typical for the streams with a higher slope value (Rosgen 1994).

Discussion

Provenance

We found a relatively monotonous garnet spectrum in the recent fluvial sediments. Already the optical evaluation of the heavy-mineral concentrates revealed two separate groups within almandine detritus. Almandines are different in size, especially in the presence/absence of chlorite-filled fractures, as well as colour shade. While the larger, often fragmented, pale-pink "cloudy" almandine grains with chlorite-filled fractures were concentrated predominantly in the samples located closer to the Krížava elevation (MFB-17 and MFB-18 samples) less throughout the entire stream profile, the smaller,

Table 2: Correlation relations between chemically induced features developed on almandine surfaces to each other.

	oriented etch pits	solution pits	solution crevasses
oriented etch pits	1		
solution pits	−0.485	1	
solution crevasses	0.366	0.094	1
facets	0.441	−0.526	−0.175

clear, pink grains containing tiny dark inclusions were distributed especially in the middle and lower section of the Stránsky potok brook, and unambiguously prevail in all of the samples studied. This optical difference is also reflected in their chemical composition, i.e., larger grains in the upper part of the stream are commonly spessartine-rich, whilst the grossular molecule is identical to the other analysed almandines. Although, their Raman spectra are very similar (Fig. 4C).

In the study of synthetic solid solution binaries of almandine–spessartine (Kolesov & Geiger 1998), only very small changes in the spectra related to the change in composition were observed in the Raman spectra of samples with an almandine content between 60 and 70 mol%. This is likely due to the similar size and mass of the Mn^{2+} and Fe^{2+} cations (Hofmeister & Chopelas 1991). In our garnet grains (MFB-18 sample), the spessartine content is significantly lower than in the given study (Kolesov & Geiger 1998); therefore, we can assume a negligible effect of spessartine on the Raman spectrum of almandine.

In the Raman spectra collected for the synthetic almandine–pyrope binary solid solutions, Raman vibration mode assignments indicate that the mode frequencies of Si–O stretching, Si–O bending, and the rotation of the SiO_4-tetrahedron decrease linearly, while the translational modes of the SiO_4-tetrahedron increase with increasing almandine content (Kuang et al. 2019). However, like the almandine–spessartine binary solid solution, the changes between the spectra with almandine content between 60 and 70 mol% are minimal in the case of the almandine–pyrope binary solid solution. It is also essential to consider that the pyrope contents in our garnet grains (MFB-18 sample) are significantly lower. The Raman spectra of the garnet grains in the MFB-18 sample (Fig. 4C) are nearly identical because both grains have a high almandine content and a significantly lower content of the other samples compared to previously-published results (Kolesov & Geiger 1998; Kuang et al. 2019).

Such a garnet type was described by Hrdlička (2006) in metagranite (granodiorite) occurring in the northern-eastern part of the granite pluton within the Veľká Lúka segment (Fig. 1).

An optically-indistinguishable, but slightly chemically different almandine occurred in the MFB-5 sample. This detrital almandine contains slightly higher spessartine and grossular components and remarkably resembles the almandine composition known from garnet–sillimanite gneiss (cf. MF-13 sample; Janák & Lupták 1997; Fig. 5). Therefore, a part of detrital almandine was derived from the remnants of the preserved metamorphic mantle of granitic rocks. It consists of various types of paragneisses which represent the xenoliths in the Veľká Lúka granitoids. These are garnet–biotite paragneisses, garnet–sillimanite gneisses, biotite paragneisses, amphibole–biotite paragneisses, and paragneisses with graphite (Rakús et al. 1989, 1993; Janák & Lupták 1997). The listed metamorphic rocks are more abundant in the eastern slopes of the Malá Fatra crystalline massif, while in the western slopes of the Veľká Lúka segment (study area), they occur as rare lenses or xenoliths (Rakús et al. 1989, 1993). In the fluvial sediments of the Stránsky potok brook, biotite gneisses without garnet were predominantly found. In addition, we did not observe detrital almandines primarily derived from amphibolites.

In general, the chemical composition of the detrital almandines indicates their source in metagranite or diatexite (see Hrdlička 2006; Broska et al. 2022).

Since secondary hydrogarnet often associates with amphibole in tonalite and amphibolite (Fig. 2F), the amphibole could be used to identify the garnet source rocks. However, the amphibole from the tonalite notably corresponding to magnesio-hastingsite (high Na content) is often altered to actinolite (Fig. 3), although the amphibole from the amphibolite corresponds similarly to magnesio-hornblende, but is also transformed to actinolite. Surprisingly, the magnesio-hornblende, which occurs in close metaperidotite, was not found in the studied fluvial sediments (Fig. 3).

Table 3: Correlation relations between mechanically induced features developed on almandine surfaces (all studied samples) and hydrological characteristics of the Stránsky potok brook (v – water-flow velocity, depth).

	V-shaped p. marks	crescentic p. marks	conchoidal fractures	arcuate steps	straight steps	v (max)	v (mean)
V-shaped p. marks	1						
crescentic p. marks	−0.127	1					
conchoidal fractures	0.258	−0.199	1				
arcuate steps	0.092	−0.006	0.339	1			
straight steps	−0.043	0.087	−0.012	−0.271	1		
v (max)	0.288	0.101	0.283	−0.429	0.220	1	
v (mean)	0.218	0.193	0.348	−0.118	−0.281	0.772	1
depth (cm)	0.276	-0.147	0.376	−0.085	0.113	0.061	−0.109

Surface microtextures in recent fluvial systems

Chemically-induced microtextures were found in all analysed almandine samples (Fig. 6) and, interesting to note, not only in those which were collected in the place where the Stránsky potok brook flows through the Permian or Triassic siliciclastic sedimentary rocks (Geological map 2008; Fig. 1B). Since the corroded garnets are modified by mechanical features that are successively younger than the chemical ones, we can confirm the formation of chemical features outside the fluvial environment (Fig. 7C, G–J). We identified only several grains whose surfaces were either faceted or covered by the solution pits/solution crevasses without any mechanical microtextural features (Fig. 7D). Chemical microtextures are apparently: (1) a remnant of intrastratal dissolution (Morton 1979, 1987; Velbel 1984; Morton et al. 1989; Salvino & Velbel 1989; Vos et al. 2014; Dolníček et al. 2021) in the case of recycled detrital almandine secondarily derived from the siliciclastic rocks or the result of (2) corrosion caused by solutions – resorption in the rims due to interaction with other minerals (intergranular diffusion along grain boundaries in a metasedimentary environment; Janák & Lupták 1997; Dempster et al. 2017). The second option concerns the garnets derived from the surrounding metasediments or metagranites (Hrdlička 2006). (3) Etched surface could be also generated by pile up of growth steps in a hydrothermal environment (Jamtveit & Andersen 1992). "Garnet can track changes in its external environment by communicating towards the crystal's interior by means of diffusion of the effects of chemical interaction with neighbouring phases" (Carlson 2006) and adequately responds on its surface. In addition to the non-existent correlation between facets and solution crevasses (Table 2), the different habitus of the dissolved grains (Fig. 7B, C) suggests the non-uniform origin of them. Grain roughness has a limited impact on provenance interpretation (Shen et al. 2024), but usually indicates intensive recycling. Whereas rounded almandines are covered by solution crevasses, subhedral ones have facets in our samples instead .

Mechanical microtextures – mainly conchoidal fractures – are evidence of fluvial transport and a consequence of the mechanical effect of mutual grain collisions in the stream (Mahaney 2002; Vos et al. 2014; Křížek et al. 2017; Bónová et al. 2024b).

Large almandine grains are often disintegrated into smaller sharp-edged fragments conditioned by numerous chlorite-filled fractures, since the preserved ones occurred in the upper part of the stream sampling locations (MFB-18 and MFB-17 samples). In some places, the Stránsky potok brook is continuously supplied by garnets following from the grains covered only by chemically-induced microtextures (e.g., MFB-2, MFB-3 samples; Fig. 7D). These grains are mixed with those already transported from the upper section of the stream (fluvial transport is documented by fresh broken almandine fragments). Interestingly, from the MFB-4 sampling point, all analysed grains show fluvial transport traces, such as V-shaped cracks, crescentic percussion marks, and conchoidal fractures; only conchoidal fractures were recorded in the MFB-11 sample, while the chemical microtextures were absent.

Records of an ancient fluvial system

In the MFB-13 sample (the last sampling point), some almandines are rounded, and the prevailed chemical features on their surfaces suggest recycling. The previous, original rounded habitus can be observed on sharp-edged (broken) fragments (Fig. 7J). The surface of conchoidal fractures covered by fine etch pits (Fig. 7E) indicates two processes in evolution or previous transport record. This corresponds to an older, fluvial sedimentary environment, previously assumed from the cross-bedding and ripples analysis within the Lúžna Fm. (e.g., Hók 1989; Vozárová 2005) or the Stráňany Fm. siliciclastic rocks (Vozárová & Vozár 1983, 1988; Havrila & Olšavský 2015). Such grains are rather rare in our fluvial samples. Most such conchoidal fractures occurred in the contemporary Stránsky potok brook environment (Fig. 7F–H). Both of the above-mentioned almandine types are geochemically identical. It should be noted that the siliciclastics of the Lúžna Fm. have high-mineralogical maturity with zircon+tourmaline+rutile predominance in their heavy-mineral assemblages (Fejdiová 1985; Mišík & Jablonský 2000). Detrital garnet is very rare in the Lúžna Fm. siliciclastics, being described so far in the Tribeč Mts. by Vozárová et al. (2003). Moreover, the presence of detrital tourmaline of schorlitic–dravitic composition in modern fluvial sediments (the MFB-12 sample) confirms its siliciclastic, and not granitic provenance. However, many chemically-induced microtextures are typically restricted to grain rims, which are vulnerable to mechanical destruction during fluvial transport, thereby explaining the low number of old transport records.

In relation to the hydrological characteristics of the stream (mainly water-flow velocity), there is a certain connection between the formation of arcuate steps, conchoidal fractures, and water-flow velocity (Table 3); the formation of typical fluvial V-shaped percussion cracks (Mahaney & Kalm 2000; Mahaney 2002; Vos et al. 2014; Křížek et al. 2017; Itamiya et al. 2019; Bónová et al. 2024b) is statistically insignificant in our study. Although a higher percentage of V-shaped marks can be observed locally in connection with an increase of velocity (MFB-5, MFB-11 samples), these observations cannot be generalized and require further research. Due to the mechanical effect of fluvial transport, all of the previously-mentioned microtextural features formed on garnet grains, while an abrasion was entirely negligible. However, the rounding of sand gains occurs very slowly during transport in water (Garzanti 2017) as it was experimentally confirmed (e.g., Kuenen 1959; Resentini et al. 2018).

Conclusions

The following facts result from the study of modern fluvial sediments taken from an active stream located in the Malá Fatra Mountains in the Western Carpathians:

- Detrital almandine was derived primarily from metagranite (diatexite) and less so from granite roof mantle metamorphic rocks;

- The characteristic fluvial microtextures, such as the conchoidal fractures, V-shaped cracks, crescentic percussion marks formed in the contemporary stream, but also the inherited transport microtextures, which correspond to a notably old, fluvial sedimentary environment, confirmed the detrital almandine surfaces;
- The chemical features, such as facets developed on first-cycle almandines are a remnant after corrosion caused by solutions;
- The conjunct study of garnet geochemical and surface microtextural features appears to be essential to determine the source rocks and successive transport in ancient and/or recent sedimentary environments.

Acknowledgements: This study was supported by the Ministry of Education, Research, Development and Youth of the Slovak Republic under the grants VEGA No. 1/0780/24 and APVV-23-0265. The authors are grateful to Dr. Igor Broska, Dr. John S. Armstrong-Altrin, and Dr. Katarína Šarinová for their constructive comments, which improved this study immensely.

References

Andò S., Garzanti E., Padoan M. & Limonta M. 2012: Corrosion of heavy minerals during weathering and diagenesis: A catalog for optical analysis. *Sedimentary Geology 280*, 165–178. https://doi.org/10.1016/j.sedgeo.2012.03.023

Armstrong-Altrin J.S. 2020: Detrital zircon U–Pb geochronology and geochemistry of the Riachuelos and Palma Sola beach sediments, Veracruz state, Gulf of Mexico: a new insight on palaeoenvironment. *Journal of Palaeogeography* 9, 1–27. https://doi.org/10.1186/s42501-020-00075-9

Armstrong-Altrin J.S., Ramos-Vázquez M.A., Madhavaraju J., Verma S.K., Macías-Martínez K. & Martínez-Ruíz D. 2022: Quartz grain microtextures in the Boca del Cielo and Chocohuital beaches in the Mexican Pacific, Chiapas state: implication on paleoenvironment. *Arabian Journal of Geosciences* 15, 1086. https://doi.org/10.1007/s12517-022-10334-9

Bersani D., Andò S., Vignola P., Moltifiori G., Marino I.-G., Lottici P.P. & Diella V. 2009: Micro-Raman spectroscopy as a routine tool for garnet analysis. *Spectrochimica Acta Part A* 73, 484–491. https://doi.org/10.1016/j.saa.2008.11.033

Bónová K., Jafarzadeh M. & Bóna J. 2021: Depositional history of the Devonian Ilanqareh and Padeha Formations in Azarbaijan Province and Eastern Alborz (Iran): constraints from heavy-mineral microtextures. *Acta Geologica Slovaca* 13, 13–26.

Bónová K., Bóna J., Mikuš T. & Ferková A. 2024a: Heavy minerals of the aeolian sediments in the East Slovak Basin (Western Carpathians) – Implications for their origin, transport process and sedimentary history. *Aeolian Research* 66, 100897. https://doi.org/10.1016/j.aeolia.2024.100897

Bónová K., Šupinský J., Bóna J., Nováková M., Šurka J. & Barabas D. 2024b: Changes in detrital garnet grain morphology and microtextures during fluvial transport in the Western Carpathians revealed by scanning electron microscopy and 3D model analysis: Implication for paleoenvironmental reconstruction. *Sedimentary Geology* 467, 106652. https://doi.org/10.1016/j.sedgeo.2024.106652

Broska I. & Svojtka M. 2020: Early Carboniferous successive I/S granite magmatism recorded in the Malá Fatra Mountains by LA ICP-MS zircon dating (Western Carpathians). *Geologica Carpathica* 71, 391–401. https://doi.org/10.31577/GeolCarp.71.5.1

Broska I., Petrík I. & Benko P. 1997: Petrology of the Malá Fatra granitoid rocks. *Geologica Carpathica* 48, 27–37.

Broska I., Janák M., Svojtka M., Yi K., Konečný P., Kubiš M., Kurylo S., Hrdlička M. & Maraszewska M. 2022: Variscan granitic magmatism in the Western Carpathians with linkage to slab break-off. *Lithos* 412, 106589. https://doi.org/10.1016/j.lithos.2021.106589

Butek J., Spišiak J. & Milovská S. 2021: Garnet–vesuvianite equilibrium in rodingites from Dobšiná (Western Carpathians). *Minerals* 11, 189. https://doi.org/10.3390/min11020189

Carlson W.D. 2006: Rates of Fe, Mg, Mn, and Ca diffusion in garnet. *American Mineralogist* 91, 1–11. https://doi.org/10.2138/am.2006.2043

Chew D., O'Sullivan G., Caracciolo L., Mark C. & Tyrrell S. 2020: Sourcing the sand: Accessory mineral fertility, analytical and other biases in detrital U–Pb provenance analysis. *Earth-Science Reviews* 202, 103093. https://doi.org/10.1016/j.earscirev.2020.103093

Delgado L.C., Kasper-Zubillaga J.J., Martínez-Serrano R.G., Ramírez M.A.C., Arellano-Torres E. & Zavala J.L. S. 2025: Source-to-sink history of detrital garnet from coastal dune sands in SW Mexico. *Geosystems and Geoenvironment* 4, 100381. https://doi.org/10.1016/j.geogeo.2025.100381

Dempster T.J., Symon S. & Chung P. 2017: Intergranular diffusion rates from the analysis of garnet surfaces: Implications for metamorphic equilibration. *Journal of Metamorphic Geology* 35, 585–600. https://doi.org/10.1111/jmg.12247

Dianiška I., Broska I., Hrdlička M., Kubiš M. & Uher P. 2002: Petrography, mineralogy and geochemistry of the Malá Fatra plutonic rocks (Višňové – Dubná Skala tunnel profile). *Manuscript, Geofond*, Bratislava, 1–68 (in Slovak).

Diella V., Bocchio R., Marinoni N., Caucia F., Spalla M.I., Adamo I., Langone A. & Mancini L. 2019: Garnets from Val d'Ala rodingites, Piedmont, Italy: An investigation of their gemological, spectroscopic and crystal chemical properties. *Minerals* 9, 728. https://doi.org/10.3390/min9120728

Dolníček Z., Krejčí Kotlánová M. & Koutňák R. 2021: Vliv diagenetických procesů na asociaci těžkých minerálů v pískovcích z lokality Slivotín (Ždánická jednotka, flyšové pásmo Vnějších Západních Karpat, Česká republika). *Bulletin Mineralogie Petrologie* 29, 27–40 (in Czech with English abstract).

Embrechts J. & Stoops G. 1982: Microscopical aspects of garnet weathering in a humid tropical environment. *Journal of Soil Science* 33, 535–545. https://doi.org/10.1111/j.1365-2389.1982.tb01787.x

Enami M. 2012: Influence of garnet hosts on the Raman spectra of quartz inclusions. *Journal of Mineralogical and Petrological Science* 107, 173–180. https://doi.org/10.2465/jmps.111216

Faryad S.W. & Dianiška I. 2003: Ti-bearing andradite–prehnite–epidote assemblage from the Malá Fatra granodiorite and tonalite (Western Carpathians). *Schweizerische Mineralogische und Petrographische Mitteilungen* 83, 47–56.

Feil S., von Eynatten H., Dunkl I., Schönig J. & Lünsdorf N.K. 2024: Inherited grain-size distributions: Effect on heavy-mineral assemblages in modern and ancient sediments. *Journal of Geophysical Research: Earth Surface* 129, e2023JF007356. https://doi.org/10.1029/2023JF007356

Fejdiová O. 1985: New information on Lower Triassic Lúžna Clastic Formation in the Central Western Carpathians. *Západné Karpaty, Séria Mineralógia, Petrografia, Geochémia, Ložiská* 10, 111–160 (in Slovak with English Resumé).

Finzel E.S. 2017: Detrital zircon microtextures and U–Pb geochronology of Upper Jurassic to Paleocene strata in the distal North American Cordillera foreland basin. *Tectonics* 36, 1295–1316. https://doi.org/10.1002/2017TC004549

Fu M., Dai J. & Zhao L. 2022: A Study on the Raman spectral characteristics of garnet from the Jiama copper polymetallic deposit in Tibet. *Minerals* 12, 1578. https://doi.org/10.3390/min12121578

Garzanti E. 2017: The maturity myth in sedimentology and provenance analysis. *Journal of Sedimentary Research* 87, 353–365. https://doi.org/10.2110/jsr.2017.17

Garzanti E., Andò S. & Vezzoli G. 2008: Settling equivalence of detrital minerals and grain-size dependence of sediment composition. *Earth and Planetary Science Letters* 273, 138–151. https://doi.org/10.1016/j.epsl.2008.06.020

Garzanti E., Andò S. & Vezzoli G. 2009: Grain-size dependence of sediment composition and environmental bias in provenance studies. *Earth and Planetary Science Letters* 277, 422–432. https://doi.org/10.1016/j.epsl.2008.11.007

Garzanti E., Resentini A., Andò S., Vezzoli G., Pereira A. & Vermeesch P. 2015: Physical controls on sand composition and relative durability of detrital minerals during ultra-long distance littoral and aeolian transport (N amibia and southern A ngola). *Sedimentology* 62, 971–996. https://doi.org/10.1111/sed.12169

Garzanti E., Andò S., Limonta M., Fielding L. & Najman Y. 2018: Diagenetic control on mineralogical suites in sand, silt, and mud (Cenozoic Nile Delta): Implications for provenance reconstructions. *Earth-Science Reviews* 185, 122–139. https://doi.org/10.1016/j.earscirev.2018.05.010

Geological map 2008: Digital Geological Map of the Slovak Republic at scale 1:50 000. *State Geological Institute of Dionýz Štúr*, Bratislava. Available online: http://apl.geology.sk/gm50js (accessed 08/2008, last update 01/2024).

Grew E.S., Locock A.J., Mills S.J., Galuskina I.O., Galuskin E.V. & Hålenius U. 2013: Nomenclature of the garnet supergroup. *American Mineralogist* 98, 785–811. https://doi.org/10.2138/am.2013.4201

Havrila M. & Olšavský M. 2015: Report on the geological mapping of the Kozol stratigraphic sequence between the Turská dolina valley and the Porubský potok stream valley. *Geologické práce, Správy* 127, 7–79 (in Slovak with English abstract).

Hawthorne F.C., Oberti R., Harlow G.E., Maresch W.V., Martin R.F., Schumacher J.C. & Welch M.D. 2012: Nomenclature of the amphibole supergroup. *American Mineralogist* 97, 2031–2048. https://doi.org/10.2138/am.2012.4276

Hofmeister A.M. & Chopelas A. 1991: Vibrational spectroscopy of end-member silicate-garnet. *Physics and Chemistry of Minerals* 17, 503–526. https://doi.org/10.1007/BF00202230

Hók J. 1989: Paleocurrent analysis and genesis of Lúžna Beds in SE part of Tribeč Mountains. *Regionálna Geológia Západných Karpát* 25, 137–141.

Hók J., Pelech O., Teťák F., Németh Z. & Nagy A. 2019: Outline of the geology of Slovakia (W. Carpathians). *Mineralia Slovaca* 51, 31–60.

Hong D., Jian X., Fu L. & Zhang W. 2020: Garnet trace element geochemistry as a sediment provenance indicator: An example from the Qaidam basin, northern Tibet. *Marine and Petroleum Geology* 116, 104316. https://doi.org/10.1016/j.marpetgeo.2020.104316

Hovorka D., Ivan P., Jaroš J., Kratochvíl M., Reichwalder P., Rojkovič I., Spišiak J. & Turanová L. 1985: Ultramafic rocks of the Western Carpathians, Czechoslovakia. *Geological Institute of Dionýz Štúr*, Bratislava, 1–258.

Hovorka D., Spišiak J. & Mikuš T. 2008: Coarse-grained hornblende–clinopyroxene–garnetiferous rocks from the Malá Fatra Mts. (Western Carpathians, Slovakia). *Mineralia Slovaca* 40, 25–32.

Hrdlička M. 2006: Granite Petrology of the Malá Fatra Mts.: Implication to the tectogenesis of collisional West-Carpathians I-type granitic suite. *PhD thesis*, *Slovak Academy of Sciences*, Bratislava, 1–147.

Itamiya H., Sugita R. & Sugai T. 2019: Analysis of the surface microtextures and morphologies of beach quartz grains in Japan and implications for provenance research. *Progress in Earth and Planetary Science* 6, 43. https://doi.org/10.1186/s40645-019-0287-9

Jamtveit B. & Andersen T.B. 1992: Morphological instabilities during rapid growth of metamorphic garnets. *Physics and Chemistry of Minerals* 19, 176–184. https://doi.org/10.1007/BF00202106

Janák M. & Lupták B. 1997: Pressure–temperature conditions of high-grade metamorphism and migmatitization in the Malá Fatra crystalline complex, the Western Carpathians. *Geologica Carpathica* 48, 287–302.

Kamenický L., Macek J. & Krištín J. 1987: Contribution to the petrography and geochemistry of the Malá Fatra granitoid rocks. *Mineralia Slovaca* 19, 311–324 (in Slovak with English summary).

Kohút M. & Larionov A.N. 2021: From subduction to collision: genesis of the Variscan granitic rocks from the Tatric Superunit (Western Carpathians, Slovakia). *Geologica Carpathica* 72, 96–113. https://doi.org/10.31577/GeolCarp.72.2.2

Kolesov B.A. & Geiger C.A. 1998: Raman spectra of silicate garnets. *Physics and Chemistry of Minerals* 25, 142–151. https://doi.org/10.1007/s00269005009

Korikovsky S.P., Kamenický L., Macek J. & Boronichin V.A. 1987: P–T conditions of metamorphism of the Malá Fatra Mts. crystalline schists (in cut of Mlynský potok brook and its surroundings). *Geologický zborník – Geologica Carpathica* 38, 409–427 (in Russian with English abstract).

Korikovsky S.P., Janák M. & Lupták B. 1998: Phase relations in olivine–orthopyroxene–chlorite–spinel–hornblende metaultramafics from the Malá Fatra Mts., Western Carpathians. *Geologica Carpathica* 49, 369–376.

Kos S., Dolenec M., Lux J. & Dolenec S. 2020: Raman microspectroscopy of garnets from S-fibulae from the archaeological site Lajh (Slovenia). *Minerals* 10, 325. https://doi.org/10.3390/min10040325

Krinsley D.H. & Doornkamp J.C. 2011: Atlas of quartz sand surface textures. *Cambridge University Press*, New York, 1–91.

Krippner A., Meinhold G., Morton A.C. & von Eynatten H. 2014: Evaluation of garnet discrimination diagrams using geochemical data of garnets derived from various host rocks. *Sedimentary Geology* 306, 36–52. https://doi.org/10.1016/j.sedgeo.2014.03.004

Krippner A., Meinhold G., Morton A.C., Russell E. & von Eynatten H. 2015: Grain-size dependence of garnet composition revealed by provenance signatures of modern stream sediments from the western Hohe Tauern (Austria). *Sedimentary Geology* 321, 25–38. https://doi.org/10.1016/j.sedgeo.2015.03.002

Krippner A., Meinhold G., Morton A. C., Schönig J. & von Eynatten H. 2016: Heavy minerals and garnet geochemistry of stream sediments and bedrocks from the Almklovdalen area, Western Gneiss Region, SW Norway: Implications for provenance analysis. *Sedimentary Geology* 336, 96–105. https://doi.org/10.1016/j.sedgeo.2015.09.009

Křížek M., Krbcová K., Mida P. & Hanáček M. 2017: Micromorphological changes as an indicator of the transition from glacial to glaciofluvial quartz grains: Evidence from Svalbard. *Sedimentary Geology* 358, 35–43. https://doi.org/10.1016/j.sedgeo.2017.06.010

Kuang Y., Xu J., Li B., Ye Z., Huang S., Chen W., Zhang D., Zhou W. & Ma M. 2019: Crystal-chemical properties of synthetic alman-

dine–pyrope solid solution by X-ray single-crystal diffraction and Raman spectroscopy. *Crystals* 19, 541. https://doi.org/10.3390/cryst9100541

Kuenen P.H. 1959: Experimental abrasion: 3. Fluviatile action on sand. *American Journal of Science* 257, 172–190.

Kurylo S. & Broska I. 2025: Formation of non-equilibrium accessory mineral paragenesis in S-/I-type granitic rocks (example from the Western Carpathians). *Chemical Geology* 667, 122625. https://doi.org/10.1016/j.chemgeo.2025.122625

Kyono A. & Arora S. 2019: Crystal structure change in grossular–Si–free katoite solid solution: Oxygen position splitting in katoite. *Journal of Mineralogical and Petrological Sciences* 114, 189–200. https://doi.org/10.2465/jmps.190424

Lager G.A., Armbruster T., Rotella F.J. & Rossman G.R. 1989: OH substitution in garnets: X-ray and neutron diffraction, infrared, and geometric-modeling studies. *American Mineralogist* 74, 840–851.

Linnemann U., Pidal A.P., Hofmann M., Drost K., Quesada C., Gerdes A., Marko L., Gärtner A., Yieger J., Ulrich J., Krause R., Vickers-Rich P. & Horak J. 2018: A ~565 Ma old glaciation in the Ediacaran of peri-Gondwanan West Africa. *International Journal of Earth Sciences* 107, 885–911. https://doi.org/10.1007/s00531-017-1520-7

Locock A.J. 2008: An Excel spreadsheet to recast analyses of garnet into end-member components, and a synopsis of the crystal chemistry of natural silicate garnets. *Computers & Geosciences* 34, 1769–1780. https://doi.org/10.1016/j.cageo.2007.12.013

Locock A.J. 2014: An Excel spreadsheet to classify chemical analyses of amphiboles following the IMA 2012 recommendations. *Computers & Geosciences* 62, 1–11. https://doi.org/10.1016/j.cageo.2013.09.011

Ma Y., Li Z., Tan D., Zou X. & Tao T. 2024: Grain size and surface micro-texture characteristics and their paleoenvironmental significance of Holocene sediment in southern margin of the Gurbantunggut Desert, China. *Journal of Arid Land* 16, 632–653. https://doi.org/10.1007/s40333-024-0015-1

Mahaney W.C. 2002: Atlas of sand grain surface textures and applications. *Oxford University Press*, USA, 1–256.

Mahaney W.C. & Kalm V. 2000: Comparative scanning electron microscopy study of oriented till blocks, glacial grains and Devonian sands in Estonia and Latvia. *Boreas* 29, 35–51. https://doi.org/10.1111/j.1502-3885.2000.tb01199.x

Malusà M.G., Resentini A. & Garzanti E. 2016: Hydraulic sorting and mineral fertility bias in detrital geochronology. *Gondwana Research* 31, 1–19. https://doi.org/10.1016/j.gr.2015.09.002

Mange M.A. & Morton A.C. 2007: Geochemistry of heavy minerals. *Developments in Sedimentology* 58, 345–391. https://doi.org/10.1016/S0070-4571(07)58013-1

Méres Š. & Hovorka D. 1989: Metamorphic development of gneisses in the Suchý, Malá Magura and Malá Fatra Mts. (Central Slovakia). *Mineralia Slovaca* 21, 203–216 (in Slovak with English abstract).

Mišík M. & Jablonský J. 2000: Lower Triassic quartzites of the Western Carpathians: transport direction, sources of clasts. *Geologica Carpathica* 51, 251–264.

Moral Cardona J., Mas J.G., Bellón A.S., Domínguez-Bella S. & López J.M. 2005: Surface textures of heavy-mineral grains: a new contribution to provenance studies. *Sedimentary Geology* 174, 223–235. https://doi.org/10.1016/j.sedgeo.2004.12.006

Morton A.C. 1979: Depth control of intrastratal solution of heavy minerals from the Palaeocene of the North Sea. *Journal of Sedimentary Research* 49, 281–286.

Morton A.C. 1987: Influences of provenance and diagenesis on detrital garnet suites in the Paleocene Forties Sandstone, central North Sea. *Journal of Sedimentary Research* 57, 1027–1032. https://doi.org/10.1306/212F8CD8-2B24-11D7-8648000102C1865D

Morton A.C. & Hallsworth C. 2007: Stability of detrital heavy minerals during burial diagenesis. *Developments in Sedimentology* 58, 215–245. https://doi.org/10.1016/S0070-4571(07)58007-6

Morton A.C., Borg G., Hansley P.L., Haughton P.D.W., Krinsley D.H. & Trusty P. 1989: The origin of faceted garnets in sandstones: dissolution or overgrowth? *Sedimentology* 36, 927–942. https://doi.org/10.1111/j.1365-3091.1989.tb01754.x

Morton A.C., Whitham A.G. & Fanning C.M. 2005: Provenance of Late Cretaceous to Paleocene submarine fan sandstones in the Norwegian Sea: integration of heavy mineral, mineral chemical and zircon age data. *Sedimentary Geology* 182, 3–28. https://doi.org/10.1016/j.sedgeo.2005.08.007

Morton A.C., Ellis D., Jolley D. & Whitham A.G. 2012: The importance of an integrated approach to provenance studies. In: Rasbury E.T., Hemming S.R. & Riggs N.R. (Eds.): Mineralogical and Geochemical Approaches to Provenance. *Geological Society of America, Special Paper* 487, 1–12. https://doi.org/10.1130/2012.2487(01)

Naidu K.B., Kumar K.V., Reddy K.S.N., Rao P.G. & Sekhar C.R. 2024: Provenance of low-grossular–high-pyrope detrital garnets from beach sands of East Coast of India between Gosthani and Vamsadhara rivers. *Sedimentary Geology* 469, 106666. https://doi.org/10.1016/j.sedgeo.2024.106666

Nascimento D.L., Martinez P., Batezelli A., Ladeira F. & Corrêa L. 2022: From the micromorphology of paleoweathering fronts to paleoenvironmental analysis: A case study of the Cretaceous dune fields of Sanfranciscana Basin, Brazil. *Catena* 211, 106008. https://doi.org/10.1016/j.catena.2021.106008

Rakús M. & Hók J. 2003: Geological structure of the Kozol anticline (Lúčanská Fatra Mts., Western Carpathians). *Mineralia Slovaca* 35, 75–88 (in Slovak).

Rakús M. (Ed.), Dovina V., Elečko M., Gašparik J., Gorek J., Halouzka R., Hanáček J., Havrila M., Horniš J., Kohút M., Kysela J., Miko O., Pristaš J., Pulec M., Rojkovičová Ľ., Šucha P., Vozárová A. & Vozár J. 1989: Geological map of the Lúčanská Malá Fatra at scale 1:50 000. Manuscript, *Geological Institute of Dionýz Štúr*, Bratislava, 1–238 (in Slovak).

Rakús M. (Ed.), Elečko M., Gašparik J., Gorek J., Kalouzka R., Havrila M., Horniš J., Kohút M., Kysela J., Miko O., Pristaš J., Pulec M., Vozár J., Vozárová A. & Wunder D. 1993: Geological map of the Lúčanská Malá Fatra Mts. at scale 1:50 000. *Geological Institute of Dionýz Štúr*, Bratislava.

Resentini A., Andò S. & Garzanti E. 2018: Quantifying roundness of detrital minerals by image analysis: Sediment transport, shape effects, and provenance implications. *Journal of Sedimentary Research* 88, 276–289. https://doi.org/10.2110/jsr.2018.12

Rosgen D.L. 1994: A classification of natural rivers. *Catena* 22, 169–199. https://doi.org/10.1016/0341-8162(94)90001-9

Salvino J.F. & Velbel M.A. 1989: Faceted garnets from sandstones of the Munising Formation (Cambrian), northern Michigan: petrographic evidence for their origin by intrastratal dissolution. *Sedimentology* 36, 371–379. https://doi.org/10.1111/j.1365-3091.1989.tb00613.x

Schönig J., von Eynatten H., Tolosana-Delgado R. & Meinhold G. 2021: Garnet major-element composition as an indicator of host-rock type: a machine learning approach using the random forest classifier. *Contributions to Mineralogy and Petrology* 176, 1–21. https://doi.org/10.1007/s00410-021-01854-w

Shen X., Jian X., Zhang W. & Guan P. 2024: Grain textural bias in detrital single-mineral provenance studies. *Sedimentary Geology* 471, 106731. https://doi.org/10.1016/j.sedgeo.2024.106731

Shcherbak N.P., Cambel B., Bartnitsky E.N. & Stepanyuk L.M. 1990: U–Pb age of granitoid rock from the quarry Dubná Skala – Malá Fatra Mts. *Geologický Zborník Geologica Carpathica* 41, 407–414.

Stutenbecker L., Mark C. & Resentini A. 2024: Editorial to the special collection "controls and biasing factors in sediment generation, routing, and provenance: Models, methods, and case studies". *Journal of Geophysical Research: Earth Surface* 129, e2024JF007874. https://doi.org/10.1029/2024JF007874

Suggate S.M. & Hall R. 2014: Using detrital garnet compositions to determine provenance: a new compositional database and procedure. *Geological Society, London, Special Publications* 386, 373–393. https://doi.org/10.1144/SP386.8

Szerakowska S., Woronko B., Sulewska M.J. & Oczeretko E. 2018: Spectral method as a tool to examine microtextures of quartz sand-sized grains. *Micron* 110, 36–45. https://doi.org/10.1016/j.micron.2018.04.008

Tolosana-Delgado R., von Eynatten H., Krippner A. & Meinhold G. 2018: A multivariate discrimination scheme of detrital garnet chemistry for use in sedimentary provenance analysis. *Sedimentary Geology* 375, 14–26. https://doi.org/10.1016/j.sedgeo.2017.11.003

Velbel M.A. 1984: Natural weathering mechanisms of almandine garnet. *Geology* 12, 631–634. https://doi.org/10.1130/0091-7613(1984)12<631:NWMOAG>2.0.CO;2

Vermeesch P. 2004: How many grains are needed for a provenance study? *Earth and Planetary Science Letters* 224, 441–451. https://doi.org/10.1016/j.epsl.2004.05.037

Vos K., Vandenberghe N. & Elsen J. 2014: Surface textural analysis of quartz grains by scanning electron microscopy (SEM): From sample preparation to environmental interpretation. *Earth-Science Reviews* 128, 93–104. https://doi.org/10.1016/j.earscirev.2013.10.013

Vozárová A. 2005: Reconstruction of fluvial bars from the Lower Triassic "Buntsadstein Facies" (Lúžna Formation) in the Western Carpathians (Slovakia). *Geologica Carpathica* 56, 41–55.

Vozárová A. & Vozár J. 1983: New information on Late Paleozoic in Malá Fatra Mts. *Geologické Práce, Správy* 79, 27–54.

Vozárová A. & Vozár J. 1988: Late Paleozoic in the Western Carpathians. *Geological Institute of Dionýz Štúr*, Bratislava, 1–314.

Vozárová A., Janošov J. & Šarinová K. 2003: Tourmaline-enriched horizons in the Lower Triassic quartzose sediments from the Tribeč Mts., Tatric Unit, Western Carpathians (Slovakia). *Slovak Geological Magazine* 9, 65–75.

Warr L.N. 2021: IMA–CNMNC approved mineral symbols. *Mineralogical Magazine* 85, 291–320. https://doi.org/10.1180/mgm.2021.43

Electronic supplementary material is available online:
Supplement S1 "Representative chemical analyses of the detrital grains/minerals from the studied samples" at https://geologicacarpathica.com/data/files/supplements/GC-76-Bonova_SupplS1.xlsx